Supporting Information

Synthesis, Structural and Spectroscopic Characterization, and Reactivities of Mononuclear Cobalt(III)-Peroxo Complexes

Jaeheung Cho,[1] Ritimukta Sarangi,[2] Hye Yeon Kang,[1] Jung Yoon Lee,[1] Minoru Kubo,[3] Takashi Ogura,[3] Edward I. Solomon,[2,4] and Wonwoo Nam*[,1]

[1]Department of Bioinspired Science, Department of Chemistry and Nano Science, Center for Biomimetic Systems, Ewha Womans University, Seoul 120-750, Korea

[2]Stanford Synchrotron Radiation Lightsource, SLAC National Accelerator Laboratory, Menlo Park, California 94025, USA

[3]Picobiology Institute, Graduate School of Life Science, University of Hyogo, Hyogo 678-1297, Japan

[4]Department of Chemistry, Stanford University, Stanford, California 94305, USA

E-mail: wwnam@ewha.ac.kr

Table S1. Selected Bond Distances (Å) and Angles (°) for **1**-$(ClO_4)_2$ and **3**-$(ClO_4)_2$

	1-$(ClO_4)_2$	**3**-$(ClO_4)_2$
Co1-N1	1.982(4)	2.068(4)
Co1-N2	1.994(4)	2.015(8)
Co1-N3	2.036(6)	
N1-Co1-N2	88.16(16)	102.06(14)
N1-Co1-N3	101.27(17)	
N1-Co1-N4	101.61(17)	

Table S2. EXAFS Least Squares Fitting Results

Complex	Coordination/Path	R(Å)[a]	σ^2(Å^2)[b]	E_0 (eV)	F [c]
2	2 Co-O	1.85	323	1.81	0.16
	4 Co-N	1.99	317		
	8 Co-C[d]	2.84	393		
	24 Co-C-N[d]	3.14	382		
4	2 Co-O	1.86	341	1.50	0.17
	4 Co-N	2.01	530		
	8 Co-C[d]	2.86	549		
	24 Co-C-N[d]	3.16	473		

[a]The estimated standard deviations for the distances are in the order of ± 0.02 Å. [b]The σ^2 values are multiplied by 10^5. [c]Error is given by $\Sigma[(\chi_{obsd} - \chi_{calcd})^2 k^6]/\Sigma[(\chi_{obsd})^2 k^6]$. [d]The single scattering contribution from the 4 methyl groups were not included while the multiple scattering contributions were required to obtain a good fit. The S_0^2 factor was set at 0.8.

Table S3. Selected DFT Parameters

Model	Structural Parameters				Mayer Bond Order		Mulliken Charge
	$Co\text{-}O_1(O_2)$	$O_1\text{-}O_2$	$Co\text{-}N_1(N_2)^a$	CoO_1O_2	Co-O	O-O	Co, O_1, O_2
2	1.88 (1.88)	1.44	2.02 (2.05)	67.5	0.89 (0.89)	0.77	0.35, -0.31, -0.31
4	1.89 (1.91)	1.42	2.05 (2.10)	67.5	0.88 (0.85)	0.82	0.39, -0.29, -0.28

[a]The average of the trans $Co\text{-}N_1(N_3)$ and $Co\text{-}N_2(N_4)$ bond distances are represented by $Co\text{-}N_1$ and $Co\text{-}N_2$, respectively.

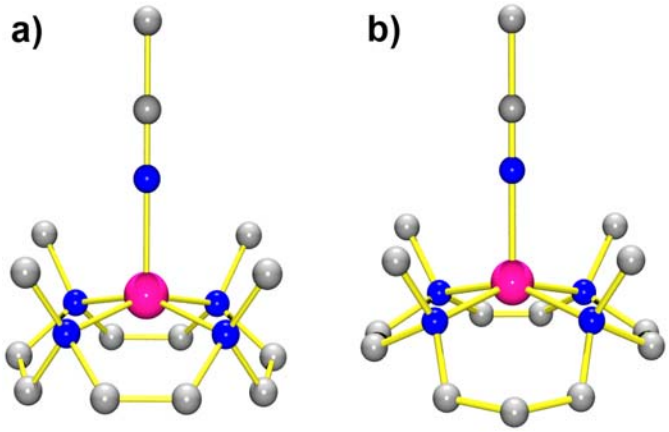

Figure S1. X-ray crystal structures of (a) $[Co(12\text{-}TMC)(CH_3CN)]^{2+}$ (**1**) and (b) $[Co(13\text{-}TMC)(CH_3CN)]^{2+}$ (**3**) (gray C, blue N, pink Co).

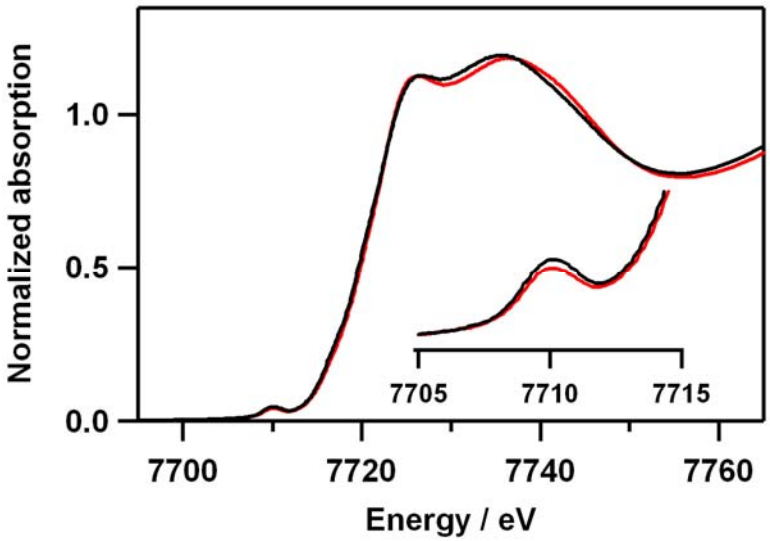

Figure S2. The normalized Co K-edge x-ray absorption spectra for **2** (—) and **4** (—). Inset shows the expanded pre-edge region.

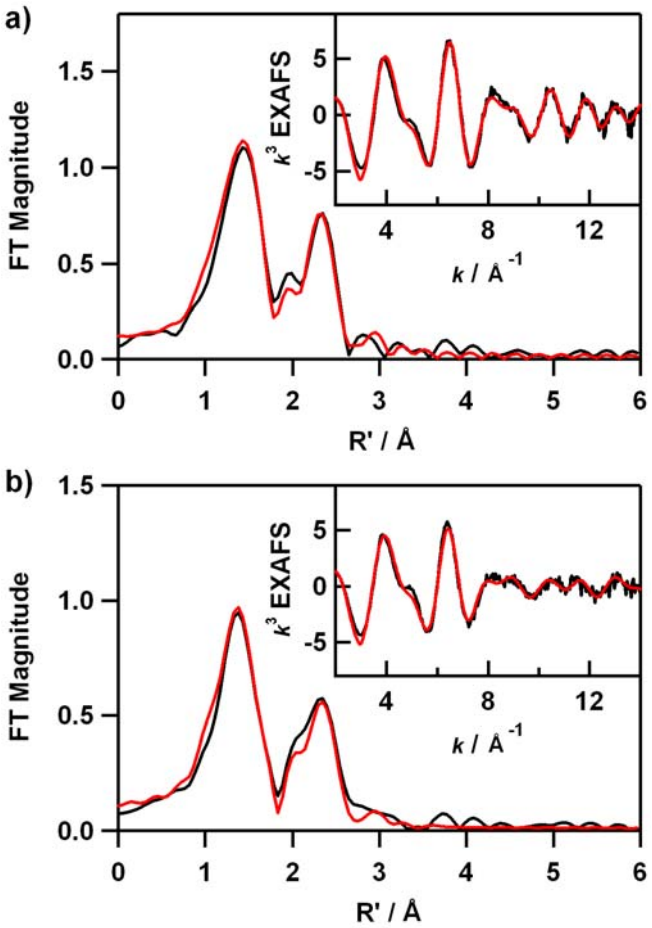

Figure S3. The k^3 weighted Co K-edge EXAFS (inset) and their corresponding non-phase shift corrected Fourier transforms for **2** (a) and **4** (b); data (—) and fit (—).

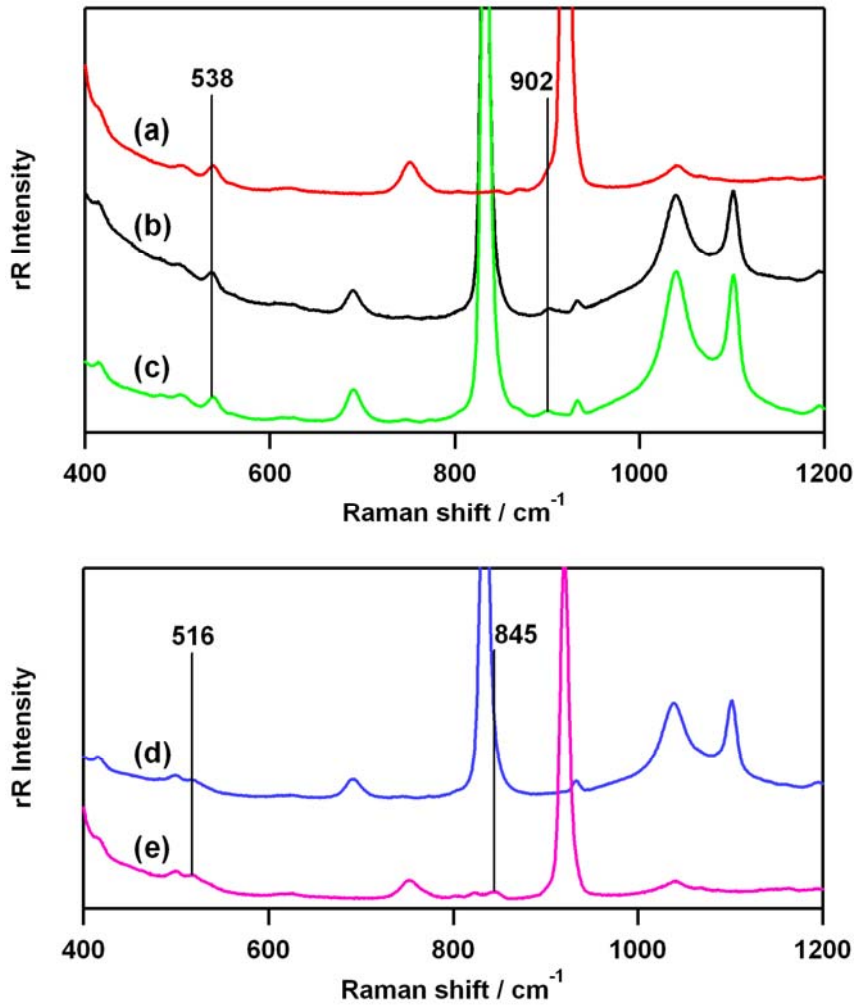

Figure S4. Resonance Raman spectra of **2**-$^{16}O_2$ (32 mM) and **2**-$^{18}O_2$ (32 mM) taken in CD_3CN and CH_3CN, respectively. (a) In situ-generated **2**-$^{16}O_2$ prepared with $H_2{}^{16}O_2$ in CH_3CN, (b) isolated **2**-$^{16}O_2$ in CD_3CN, (c) in situ-generated **2**-$^{16}O_2$ prepared with $H_2{}^{16}O_2$ in CD_3CN, (d) in situ-generated **2**-$^{18}O_2$ prepared with $H_2{}^{18}O_2$ in CD_3CN, and (e) in situ-generated **2**-$^{18}O_2$ prepared with $H_2{}^{18}O_2$ in CH_3CN. Since the ^{16}O-^{16}O stretching band at 902 cm^{-1} and the ^{18}O-^{18}O stretching band at 845 cm^{-1} were severely overlapped with the strong CH_3CN and CD_3CN solvent peaks, respectively, the resonance Raman spectra of **2**-$^{16}O_2$ and **2**-$^{18}O_2$ were taken in different solvents such as CD_3CN for **2**-$^{16}O_2$ and CH_3CN for **2**-$^{18}O_2$.

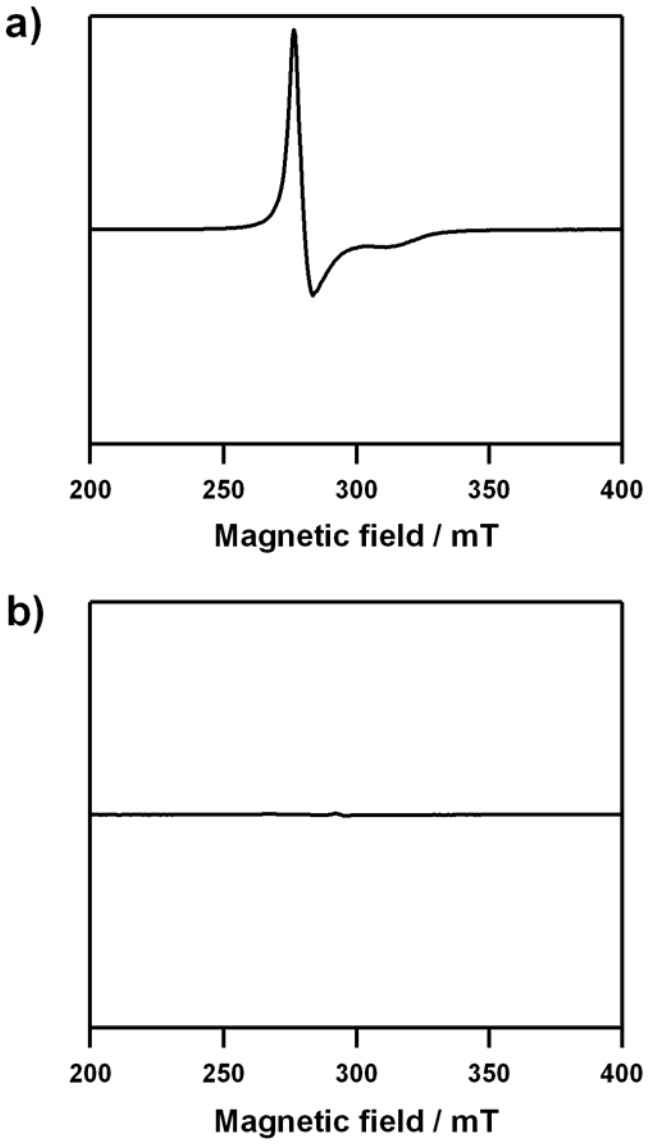

Figure S5. X-band EPR spectra of a) $[Co(12\text{-}TMC)(CH_3CN)]^{2+}$ (**1**) (g values = 2.31, 2.07) and b) $[Co(12\text{-}TMC)(O_2)]^{+}$ (**2**) in frozen CH_3CN at 4.3 K. Instrumental parameters: microwave power = 0.998 mW, frequency = 9.10 GHz, sweep width = 0.5 T, modulation amplitude = 0.2 mT.

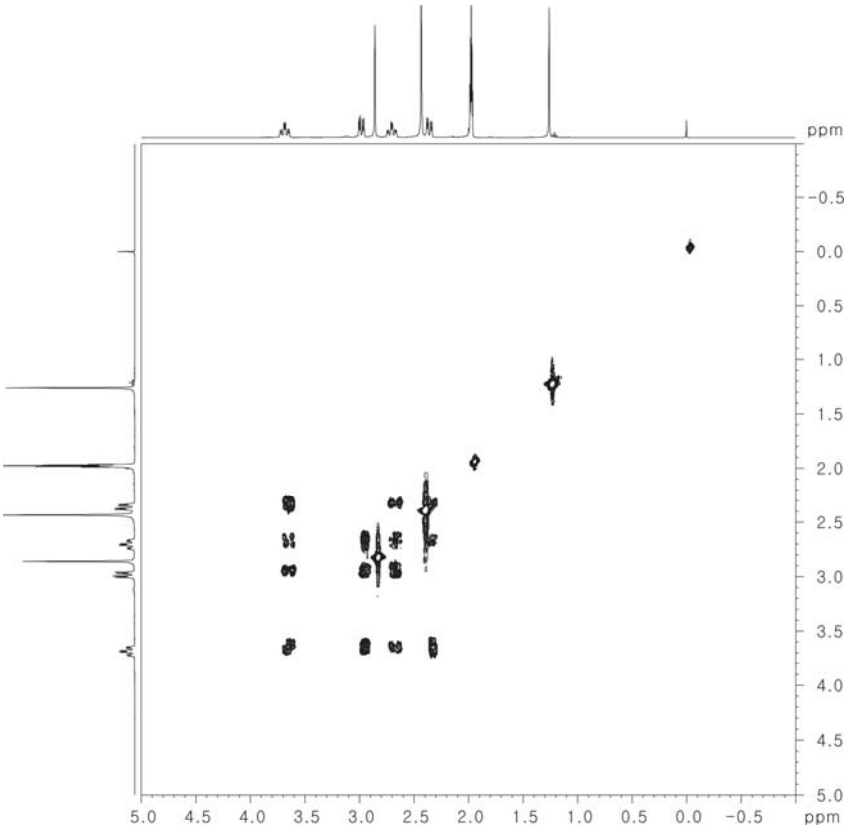

Figure S6. COSY spectrum of $[Co(12\text{-}TMC)(O_2)]^+$ (**2**) in acetonitrile-d_3 at –40 °C.

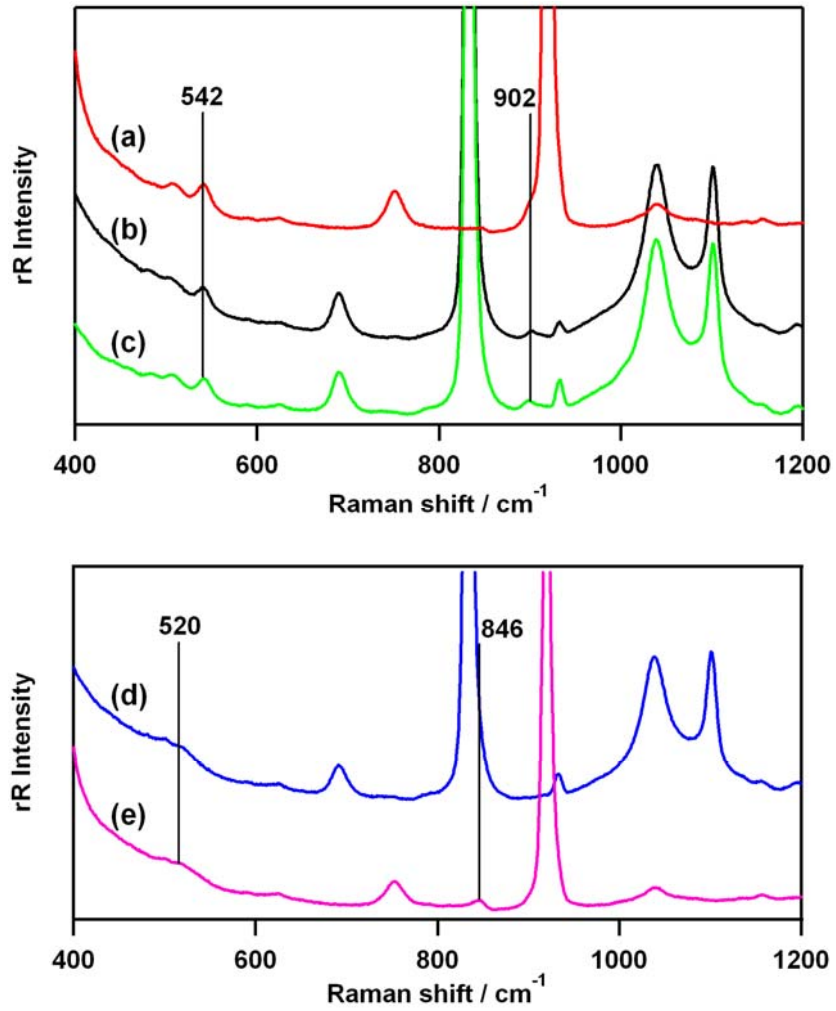

Figure S7. Resonance Raman spectra of **4**-$^{16}O_2$ (32 mM) and **4**-$^{18}O_2$ (32 mM) taken in CD_3CN and CH_3CN, respectively. (a) In situ-generated **4**-$^{16}O_2$ prepared with $H_2{}^{16}O_2$ in CH_3CN, (b) isolated **4**-$^{16}O_2$ in CD_3CN, (c) in situ-generated **4**-$^{16}O_2$ prepared with $H_2{}^{16}O_2$ in CD_3CN, (d) in situ-generated **4**-$^{18}O_2$ prepared with $H_2{}^{18}O_2$ in CD_3CN, and (e) in situ-generated **4**-$^{18}O_2$ prepared with $H_2{}^{18}O_2$ in CH_3CN. Since the ^{16}O-^{16}O stretching band at 902 cm^{-1} and the ^{18}O-^{18}O stretching band at 846 cm^{-1} were severely overlapped with the strong CH_3CN and CD_3CN solvent peaks, respectively, the resonance Raman spectra of **4**-$^{16}O_2$ and **4**-$^{18}O_2$ were taken in different solvents such as CD_3CN for **4**-$^{16}O_2$ and CH_3CN for **4**-$^{18}O_2$.

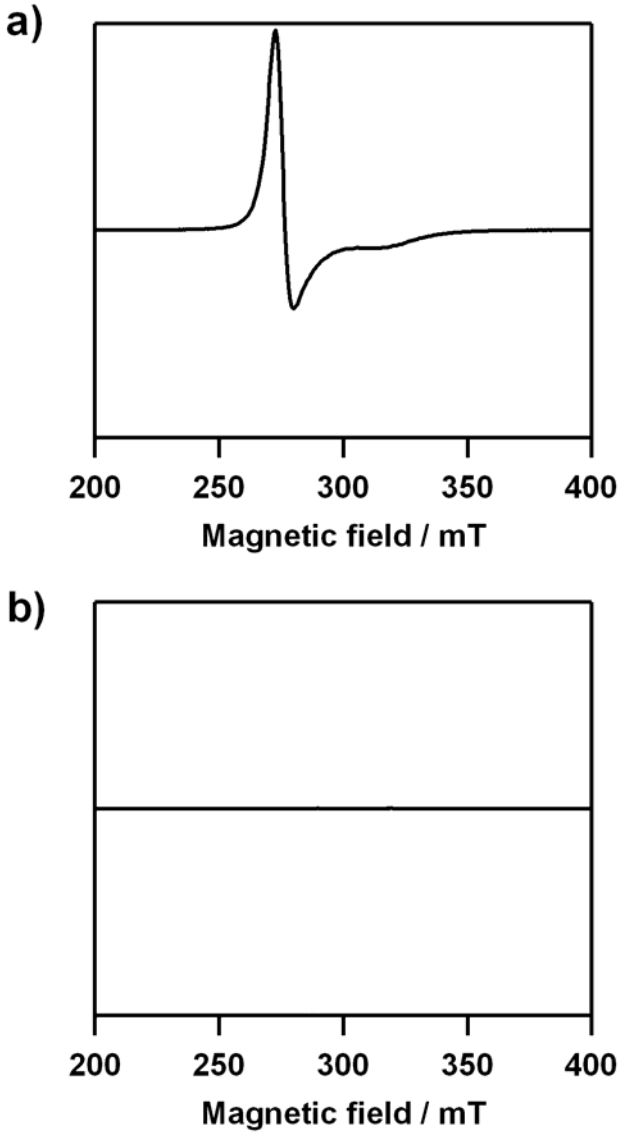

Figure S8. X-band EPR spectra of (a) $[Co(13\text{-}TMC)(CH_3CN)]^{2+}$ (**3**) (g values = 2.35, 2.05) and (b) $[Co(13\text{-}TMC)(O_2)]^{+}$ (**4**) in frozen CH_3CN at 4.3 K. Instrumental parameters: microwave power = 0.998 mW, frequency = 9.10 GHz, sweep width = 0.5 T, modulation amplitude = 0.5 mT.

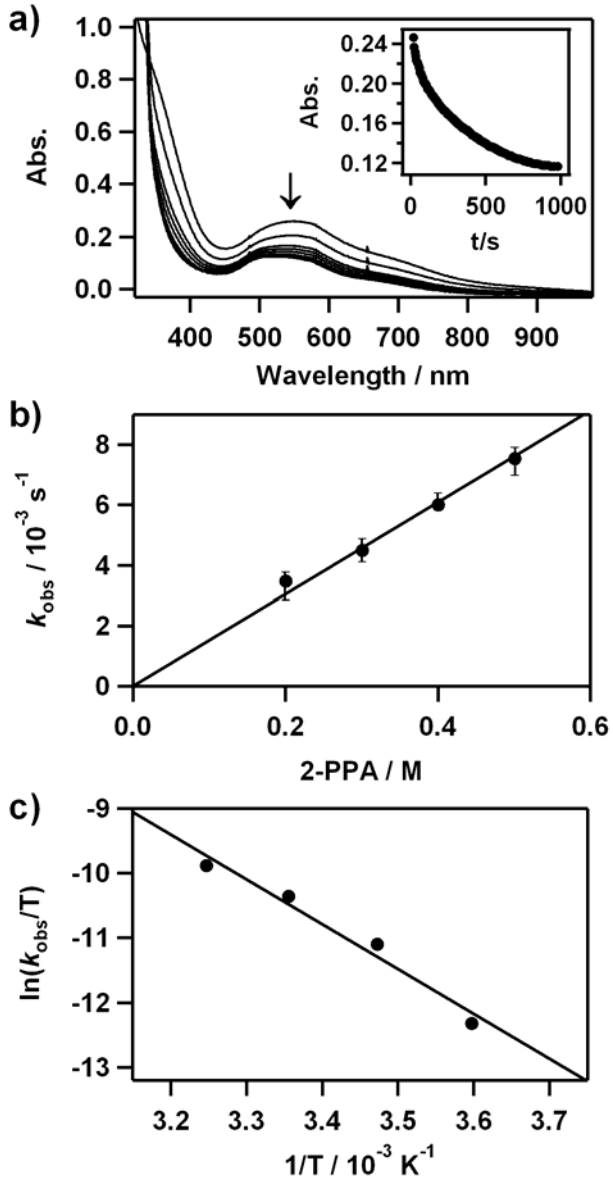

Figure S9. Reactions of $[Co(13\text{-}TMC)(O_2)]^+$ (**4**) with 2-phenylpropionaldehyde (2-PPA) in CH_3CN at 25 °C. a) UV-vis spectral changes of **4** (2 mM) upon addition of 100 equiv of 2-PPA. Inset shows the time course of the absorbance at 562 nm. b) Plot of k_{obs} against 2-PPA concentration to determine a second-order rate constant. c) Plot of first-order rate constants against 1/T to determine activation parameters for the reaction of **4** (2 mM) and 100 equiv of 2-PPA.

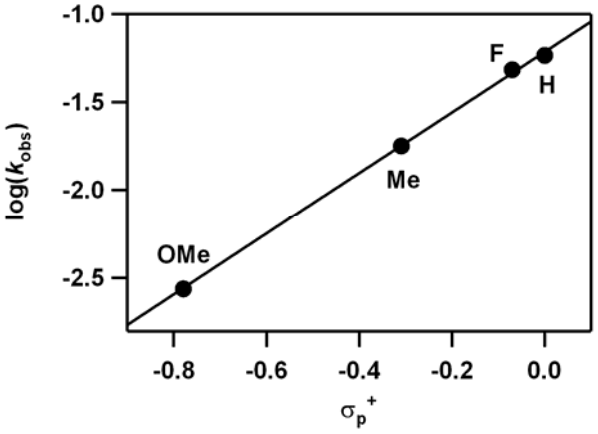

Figure S10. Hammett plot for the oxidation of *para*-substituted benzaldehydes, *para*-X-Ph-CHO (X = OMe, Me, F, H), by $[Co(13\text{-}TMC)(O_2)]^+$ (**4**) in CH_3CN at 25 °C

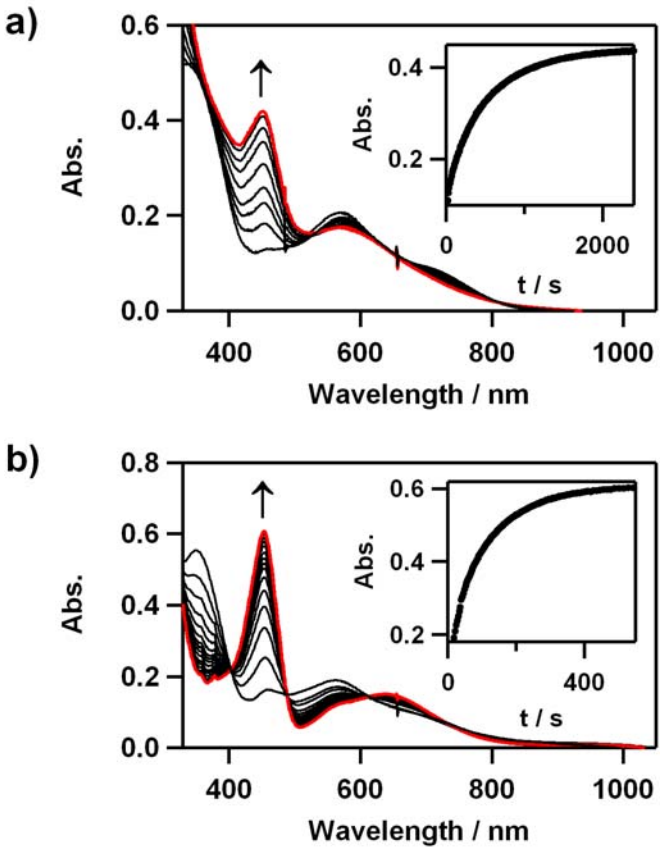

Figure S11. a) UV-vis spectral changes of $[Co(12\text{-}TMC)(O_2)]^+$ (**2**) (1 mM) upon addition of 15 equiv $[Mn(14\text{-}TMC)]^{2+}$ in acetone at 0 ºC. Inset shows the time course of the absorbance at 453 nm. b) UV-vis spectral changes of $[Co(13\text{-}TMC)(O_2)]^+$ (**4**) (1 mM) upon addition of 10 equiv $[Mn(14\text{-}TMC)]^{2+}$ in acetone at –30 ºC. Inset shows the time course of the absorbance at 453 nm.